JACS JOURNAL OF THE AMERICAN CHEMICAL SOCIETY

Communication

Cite This: J. Am. Chem. Soc. 2018, 140, 12310−12313

pubs.acs.org/JACS

Identification of PAmKate as a Red Photoactivatable Fluorescent Protein for Cryogenic Super-Resolution Imaging

Peter D. Dahlberg,[†] Annina M. Sartor,[†] Jiarui Wang,[†,‡] Saumya Saurabh,[‡] Lucy Shapiro,[‡] and W. E. Moerner*[,†]

[†]Department of Chemistry, Stanford University, Stanford, California 94305, United States

[‡]Department of Developmental Biology, Stanford University School of Medicine, Stanford, California 94305, United States

Supporting Information

ABSTRACT: Single-molecule super-resolution fluorescence microscopy conducted in vitrified samples at cryogenic temperatures offers enhanced localization precision due to reduced photobleaching rates, a chemical-free and rapid fixation method, and the potential of correlation with cryogenic electron microscopy. Achieving cryogenic super-resolution microscopy requires the ability to control the sparsity of emissive labels at cryogenic temperatures. Obtaining this control presents a key challenge for the development of this technique. In this work, we identify a red photoactivatable protein, PAmKate, which remains activatable at cryogenic temperatures. We characterize its activation as a function of temperature and find that activation is efficient at cryogenic and room temperatures. We perform cryogenic super-resolution experiments *in situ*, labeling PopZ, a protein known to assemble into a microdomain at the poles of the model bacterium *Caulobacter crescentus*. We find improved localization precision at cryogenic temperatures compared to room temperature by a factor of 4, attributable to reduced photobleaching.

Super-resolution fluorescence microscopy is a powerful technique to specifically label cellular components of interest and observe their spatial organization with ∼20−40 nm resolution.[1] This resolution enhancement beyond the ∼250 nm diffraction limit has provided a wealth of new biological insight. In single-molecule variants of super-resolution microscopy, such as PALM or STORM, the localization precision of a single emitter is inversely proportional to the square root of the number of collected photons before photobleaching occurs.[2] It is well-known that the photobleaching rate for many fluorescent proteins and small molecules is decreased at cryogenic temperatures, allowing for the collection of more photons and therefore enhanced localization precision.[3] Additionally, with vitrified sample preparation based on rapid plunge freezing, cryogenic super-resolution offers a superior alternative to chemical fixation, and the images produced can be correlated with cryogenic electron microscopy.[4] The decreased photobleaching rate has already been used to great success in sparse single-molecule cryogenic studies to achieve subnanometer localization precision.[5,6] However, unlike in single-molecule studies, super-resolution imaging requires a high labeling density and control of the emitter concentration. The majority of the fluorescent labels at any given time must be in a nonemissive state, allowing the point spread function of the few labels in an emissive state to be observed and localized free from overlap of neighboring emitters. The ability to actively control the emissive state of fluorescent labels at cryogenic temperatures, where thermally activated pathways are absent, presents a key challenge to the development of cryogenic super-resolution imaging.

To date, few fluorescent proteins and no small molecules have been reported to possess robust control mechanisms for activation at cryogenic temperatures.[4,7−9] Little characterization has been reported of how well these activation mechanisms function at cryogenic temperatures compared to their function at room temperature (RT), and conflicting reports exist on the activation capability of certain fluorescent proteins.[4,9] In this work, we identify PAmKate, a red photoactivatable protein,[10] as maintaining robust activation at cryogenic temperatures. We characterize its activation efficiency at 77 K and demonstrate its potential for cryogenic super-resolution experiments in the model bacterium *Caulobacter crescentus*.

PAmKate is the photoactivatable derivative of the monomeric fluorescent protein mKate,[10] which itself was derived from TurboRFP.[11] Recombinant PAmKate protein was isolated from BL21 *Escherichia coli* (Addgene plasmid #32691).[10] The cryogenic excitation and emission spectra of isolated and photoactivated PAmKate are shown in Figure 1A. The 628 nm emission peak at RT shifts to 616 nm at 77 K, with a concomitant narrowing of the line widths at 77 K, showing the vibronic shoulder which is not discernible at RT.

The exact photoactivation pathway for PAmKate from its dark state to its active state is unknown. However, the mechanism is suspected to consist of a transition from a neutral DsRed-like chromophore to its anionic fluorescent form following deprotonation and decarboxylation induced by absorption of 405 nm light.[10,12] It is unclear whether this proposed mechanism applies at cryogenic temperatures; however, PAGFP has been shown to activate at cryogenic temperatures[4] and is proposed to have a similar mechanism of activation and chromophore structure to PAmKate.[12] Crystal structures of the inactive and active PAGFP (PDB 3GJ1, 3GJ2) show little rearrangement of the overall protein

Received: June 15, 2018
Published: September 17, 2018

DOI: 10.1021/jacs.8b05960
J. Am. Chem. Soc. 2018, 140, 12310−12313

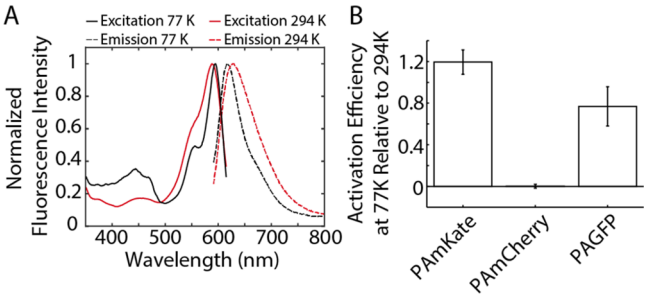

Figure 1. (A) Fluorescence excitation and emission spectra of PAmKate in 70:30 glycerol:phosphate buffered saline pH 7.4 at RT and 77 K. Excitation at 561 nm, emission detected at 635 nm. (B) Bulk activation efficiencies of PAmKate, PAmCherry, and PAGFP at 77 K compared to their activation efficiencies at RT. Error bars represent the standard error of the mean from multiple fields of view.

structure during activation.[13] While it is likely that large structural rearrangements on the excited state manifold hinder activation at cryogenic temperatures, it is not clear that large rearrangements are always prohibited or that rational fluorophore choices can be made based solely on such rearrangements. For example, PAmCherry, which is known to rely on a *cis*−*trans* isomerization when transitioning into the bright state at RT,[12] has been reported as nonphotoactivatable under cryogenic conditions.[4] The isomerization in its activation pathway involves large structural rearrangements for both the fluorophore as well as the surrounding amino acid residues.[14] However, work on the reversibly photoswitchable fluorescent protein Padron demonstrated a *cis*−*trans* isomerization at 100 K and suggests that, instead, a solvent-mediated protonation of the chromophore prevents its activation below the protein glass transition temperature of 180 K.[15]

Given the potential for thermal barriers in the activation process, it is informative to determine the activation efficiency at cryogenic temperatures compared to RT. In addition to PAmKate, we tested PAGFP and PAmCherry to provide a positive and negative control, respectively. We developed a two part assay to determine the activation efficiency at cryogenic temperatures for the three proteins. First, the brightness of single emitters at RT and 77 K was characterized. Second, the fluorescence intensity change upon activation was assessed at RT and 77 K. The intensity change was then scaled by the brightness of single emitters to quantify the number of emitters per unit area activated for a given activation pulse.

To assess single-emitter brightness, nanomolar concentrations of preactivated purified protein (SI) were mixed 1:4 v/v with 1% MOWIOL 4-88 (Polysciences Inc.) in nanopure water, dropcast onto glow-discharged electron microscopy grids (Electron Microscopy Sciences CF200F1-Cu) and air-dried. These grids were imaged on a cryostage (Linkam Scientific CMS196) using a long working distance objective (Nikon CFI TU Plan Apo 100x/NA0.9) mounted on a custom upright microscope first at RT and then at 77 K. Fluorescence images were recorded with an EMCCD camera (Andor iXon) and the brightness of single emitters was measured at both temperatures. Excitation was performed using 488 nm light for PAGFP and 561 nm light for PAmKate and PAmCherry (CrystaLaser). Excitation powers were kept low (~100 W/cm^2) to avoid sample heating. In all cases, the average brightness of single emitters varied by less than 25% between 294 and 77 K (Figure S1).

To characterize the photoactivation, BL21 cells expressing each protein in the cytoplasm were imaged at RT and at 77 K. Cells were induced for 3 h with either 1 mM IPTG or 1% arabinose to express the respective proteins. A 3 μL aliquot of each cell culture was plunge frozen (Gatan CP3) on holey carbon electron microscopy grids (Quantifoil R2/2 on Cu G200F1) for imaging at 77 K, and another similar sized aliquot was placed on an agarose pad for imaging at RT. During fluorescence imaging, the cells were activated with 50−500 ms pulses of 405 nm light (Coherent Obis) at 5−15 W/cm^2. For each protein, the activation conditions were kept uniform between temperatures. The number of activated proteins per unit area was determined from the change in intensity upon activation scaled by the average single-emitter brightness determined earlier in the *in vitro* assay. Figure S2 shows a representative activation of PAmKate at 77 K and the workflow for the activation assay.

While PAmCherry shows no significant photoactivation at 77 K, the activation efficiencies of both PAGFP and PAmKate at 77 K are comparable to their efficiency at RT (Figure 1B and Table S1). This finding suggests that, following absorption of 405 nm light, there is no subsequent large energy barrier in the process of activation for either PAmKate or PAGFP.

To test the applicability of PAmKate for cryogenic super-resolution fluorescence microscopy, we created its fusion with a previously characterized protein, PopZ, in the bacterium *Caulobacter crescentus*. PopZ is known to accumulate at the poles of *C. crescentus* as scaffolds with size scales below the diffraction limit.[16,17] *C. crescentus* cells expressing inducible PAmKate-PopZ fusions (SI) were induced with 0.3% xylose for 3 h during log phase. A 3 μL volume of cell culture was plunge frozen on a holey carbon finder grid and imaged using the cryogenic microscope described above. The 561 nm light used for fluorescence readout was maintained at 100 W/cm^2 to avoid sample devitrification. Photoactivation was performed with 10 W/cm^2 of 405 nm light for 100 ms approximately every 64 s. 10 000 frames were acquired at 1 Hz over the region shown in Figure 2 and Figures S3 and S4.

Owing to reduced photobleaching at cryogenic temperatures and the limited excitation intensities used, individual PAmKate proteins remained in the fluorescent state for many seconds or minutes. Due to these long on-times, the 1 s frames could be binned into 5 s frames following removal of activation frames and drift correction (Movie S1 and Figure S5). These binned data were processed using ThunderSTORM, an ImageJ plugin (SI).[19] Figure 2A shows a 2D histogram (red) of the number of localizations overlaid on top of a white light image of the same field of view. Because each PAmKate has many on-frames, this representation severely overcounts the number of emitters. Therefore, localizations were grouped based on their proximity in time and space (SI). These grouped localizations are our best estimate of individual emitter locations and are represented as gold circles in Figure 2B. An exact spatial extent of the PopZ domain is difficult to ascertain from the sparse localizations displayed in Figure 2B. However, the domain size is consistent with previous electron microscopy[16] and super-resolution[17] data that suggest the domain is a 100−300 nm hemispherical region. The emitters represented by the gold circles show single-step bleaching dynamics (Figure 2C,D), as expected for single proteins. Incredibly, under these conditions, single proteins can be emissive for up to 20 min before photobleaching, allowing 1.6 million photons to be collected, yielding a localization precision of 0.8 nm as measured by

DOI: 10.1021/jacs.8b05960
J. Am. Chem. Soc. 2018, 140, 12310−12313

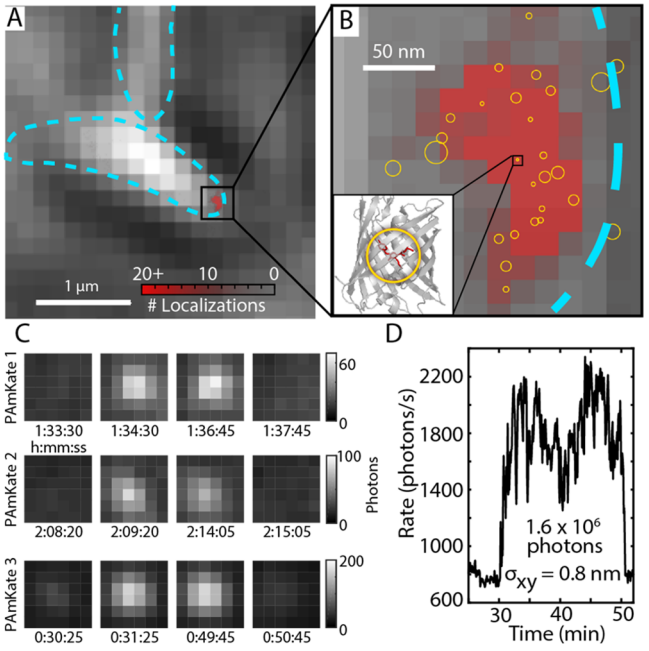

Figure 2. (A) White light image of plunge-frozen *C. crescentus* cells imaged at 77 K, outlined in blue. Overlaid in red is a 2D histogram of localizations generated from the super-resolution reconstruction. The colorbar of the histogram is truncated at 20 to make pixels with few localizations visible. (B) Zoom in of the cell pole indicated by the black square in panel A. Gold circles are centered on the average of grouped frame localizations with radii equivalent to the standard error of the mean. These circles represent the best estimate of single-emitter locations. Inset shows the grouped localization precision in the black square to scale with mKate crystal structure (PDB 3BXB[18]) (C). Three representative single PAmKate molecules over time. All show single-step activation and single-step bleaching. PAmKate 3 corresponds to the localization in the black square in panel B. (D) Raw intensity time trace associated with boxed localization in panel B and PSF shown as PAmKate 3 in panel C. Intensity is the result of integrating the 5 × 5 pixel region centered on the localization.

taking the standard error of the mean of molecular positions over all frames in which the molecule was detected (SI). At these extreme length scales, numerous effects that are not yet rigorously accounted for in this work will influence the accuracy of the localization. For instance, optical aberrations, camera pixel heterogeneity,[20] and even the distance between the probe and the protein of interest can all cause systematic errors on the nanometer scale. While fixed dipole orientation is known to cause significant systematic localization errors for molecules displaced from the focal plane,[21] in the case of the low NA collection optics used here and near-in-focus imaging through the low index material, this effect is negligible.[5]

For comparison of localization precision, the same *C. crescentus* strain was imaged on agarose pads using a conventional super-resolution setup at RT (SI). Excitation at 561 nm was performed at 240 W/cm^2 and activation was achieved with one second pulses of 405 nm light at 20 W/cm^2 (Movie S2). Figure S6 shows the RT super-resolution reconstruction for a field of view containing several cells. Localizations were again grouped (SI), and the distribution of collected photons and the resulting localization precision per grouped emitter are shown in Figure 3 for both RT and 77 K data sets. Because emitters were typically only on for a single frame in the RT data, the localization precision was calculated rather than experimentally determined by the standard error of

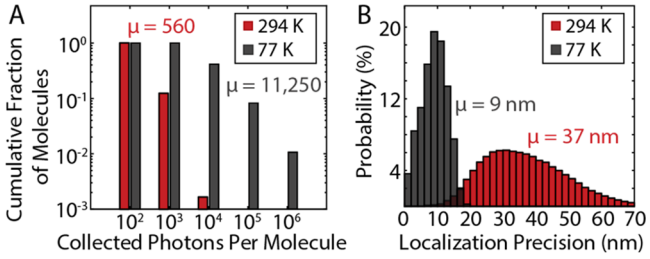

Figure 3. (A) Distribution of collected photons from super-resolution imaging of PAmKate-PopZ fusions at RT and 77 K after grouping localizations. (B) Distribution of localization precisions from super-resolution imaging of PAmKate-PopZ fusions at RT and 77 K again after grouping.

the mean position as in the 77 K data set.[22] The average number of collected photons per grouped PAmKate localization improved 20-fold under cryogenic conditions despite the reduced NA of the air objective. Consistent with this increase in photons, localization precision improved more than 4-fold. For approximately 8% of the PAmKate molecules at 77 K, more than 100 000 photons were collected. For these high photon emitters, the average localization precision was just 1.4 nm.

While this localization precision may be impressive, the long on-times of single molecules at 77 K also pose a challenge for conducting cryogenic super-resolution imaging. These long on-times make it likely that multiple molecules emit simultaneously in the same diffraction limited volume, resulting in overlapping PSFs from multiple emitters. Avoiding this problem requires careful modulation of excitation and activation parameters and, in general, slow imaging and drift reduction. While some amount of overlap may be managed computationally, future ideal fluorophores for cryogenic single-molecule imaging will require improved control mechanisms for both directions of the transition between off and on states within the constraints on illumination intensity required to prevent sample devitrification. This improved control will help prevent overlapping emitters and enable increased sampling density. Despite these current limitations, this method provides enhanced localization precision beyond RT super-resolution and does so in a manner compatible with cryogenic electron microscopy. Future correlative studies will be able to use PAmKate fusions to specifically mark molecules of interest, providing a ground truth identification of a position with a precision comparable to that of cryogenic electron microscopy resolution.

■ ASSOCIATED CONTENT

Supporting Information

The Supporting Information is available free of charge on the ACS Publications website at DOI: 10.1021/jacs.8b05960.

Details on the purification of photoactivatable proteins, generation of the *C. crescentus* strain, super-resolution data acquisition, ThunderSTORM processing (PDF)

Movie showing sample of cryogenic single-molecule imaging data, post drift correction and removal of activation frames (AVI)

Movie showing sample of RT single-molecule imaging data, post drift correction and removal of activation frames (AVI)

DOI: 10.1021/jacs.8b05960
J. Am. Chem. Soc. 2018, 140, 12310−12313

AUTHOR INFORMATION

Corresponding Author

*wmoerner@stanford.edu

ORCID

W. E. Moerner: 0000-0002-2830-209X

Notes

The authors declare no competing financial interest.

ACKNOWLEDGMENTS

This work was supported in part by the National Institute of General Medical Sciences Grant Nos. R35GM118067 (to W.E.M.) and R35GM118071 (to L.S.). J.W. is a Stanford Center for Molecular Analysis and Design Fellow. L.S. is a Chan Zuckerberg Biohub Investigator.

REFERENCES

(1) Sahl, S. J.; Moerner, W. E. *Curr. Opin. Struct. Biol.* **2013**, *23*, 778−787.

(2) Thompson, R. E.; Larson, D. R.; Webb, W. W. *Biophys. J.* **2002**, *82*, 2775−2783.

(3) Moerner, W. E.; Orrit, M. *Science* **1999**, *283*, 1670−1676.

(4) Chang, Y. W.; Chen, S.; Tocheva, E. I.; Treuner-Lange, A.; Lobach, S.; Sogaard-Andersen, L.; Jensen, G. J. *Nat. Methods* **2014**, *11*, 737−739.

(5) Weisenburger, S.; Jing, B.; Hänni, D.; Reymond, L.; Schuler, B.; Renn, A.; Sandoghdar, V. *ChemPhysChem* **2014**, *15*, 763−770.

(6) Weisenburger, S.; Boening, D.; Schomburg, B.; Giller, K.; Becker, S.; Griesinger, C.; Sandoghdar, V. *Nat. Methods* **2017**, *14*, 141.

(7) Kaufmann, R.; Schellenberger, P.; Seiradake, E.; Dobbie, I. M.; Jones, E. Y.; Davis, I.; Hagen, C.; Grünewald, K. *Nano Lett.* **2014**, *14*, 4171−4175.

(8) Nahmani, M.; Lanahan, C.; DeRosier, D.; Turrigiano, G. G. *Proc. Natl. Acad. Sci. U. S. A.* **2017**, *114*, 3832.

(9) Liu, B.; Xue, Y.; Zhao, W.; Chen, Y.; Fan, C.; Gu, L.; Zhang, Y.; Zhang, X.; Sun, L.; Huang, X.; Ding, W.; Sun, F.; Ji, W.; Xu, T. *Sci. Rep.* **2015**, *5*, 13017.

(10) Gunewardene, M.; Subach, F.; Gould, T.; Penoncello, G.; Gudheti, M.; Verkhusha, V.; Hess, S. *Biophys. J.* **2011**, *101*, 1522−1528.

(11) Shcherbo, D.; Merzlyak, E. M.; Chepurnykh, T. V.; Fradkov, A. F.; Ermakova, G. V.; Solovieva, E. A.; Lukyanov, K. A.; Bogdanova, E. A.; Zaraisky, A. G.; Lukyanov, S.; Chudakov, D. M. *Nat. Methods* **2007**, *4*, 741.

(12) Shcherbakova, D. M.; Verkhusha, V. V. *Curr. Opin. Chem. Biol.* **2014**, *20*, 60−68.

(13) Henderson, J. N.; Gepshtein, R.; Heenan, J. R.; Kallio, K.; Huppert, D.; Remington, S. J. *J. Am. Chem. Soc.* **2009**, *131*, 4176−4177.

(14) Subach, F. V.; Malashkevich, V. N.; Zencheck, W. D.; Xiao, H.; Filonov, G. S.; Almo, S. C.; Verkhusha, V. V. *Proc. Natl. Acad. Sci. U. S. A.* **2009**, *106*, 21097−21102.

(15) Regis Faro, A.; Carpentier, P.; Jonasson, G.; Pompidor, G.; Arcizet, D.; Demachy, I.; Bourgeois, D. *J. Am. Chem. Soc.* **2011**, *133*, 16362−16365.

(16) Bowman, G. R.; Comolli, L. R.; Gaietta, G. M.; Fero, M.; Hong, S.; Jones, Y.; Lee, J. H.; Downing, K. H.; Ellisman, M. H.; McAdams, H. H.; Shapiro, L. *Mol. Microbiol.* **2010**, *76*, 173−189.

(17) Gahlmann, A.; Ptacin, J. L.; Grover, G.; Quirin, S.; von Diezmann, A. R. S.; Lee, M. K.; Backlund, M. P.; Shapiro, L.; Piestun, R.; Moerner, W. E. *Nano Lett.* **2013**, *13*, 987−993.

(18) Pletnev, S.; Shcherbo, D.; Chudakov, D. M.; Pletneva, N.; Merzlyak, E. M.; Wlodawer, A.; Dauter, Z.; Pletnev, V. *J. Biol. Chem.* **2008**, *283*, 28980−28987.

(19) Ovesny, M.; Krizek, P.; Borkovec, J.; Svindrych, Z.; Hagen, G. M. *Bioinformatics* **2014**, *30*, 2389−2390.

(20) Pertsinidis, A.; Zhang, Y.; Chu, S. *Nature* **2010**, *466*, 647−651.

(21) Backlund, M. P.; Lew, M. D.; Backer, A. S.; Sahl, S. J.; Moerner, W. E. *ChemPhysChem* **2014**, *15*, 587−599.

(22) Quan, T.; Zeng, S.; Huang, Z.-L. *J. Biomed. Opt.* **2010**, *15*, 066005.

DOI: 10.1021/jacs.8b05960
J. Am. Chem. Soc. 2018, 140, 12310−12313